Analysis of Re-Entry Vehicle Behavior during Boundary-Layer Transition

G. T. CHRUSCIEL*
Lockheed Missiles and Space Company, Inc., Sunnyvale, Calif.

Analysis of re-entry vehicle (RV) behavior during the period of boundary-layer transition is performed using the full three degree of rotational freedom plane fixed equations of motion without limitations of linearizations or quasi-steady restrictions. Flight data for a number of RVs, including ablative and nonablative afterbodies, showed large divergencies in the magnitude and sense of the precession characteristics. Associated with the large excursions in the precession behavior are significant changes in the character of the motion, i.e., the ratio of maximum to minimum angle of attack. Three possible sources of these anomalies were investigated: unstable damping; static "out-of-plane" moments; "in-plane" static moment asymmetries. Analyses show the unstable damping postulation is highly improbable; simulations employing "out-of-plane" static moments adequately describe the majority of flight results. However, significant discrepancies are noted for two flights. A rapidly varying body fixed moment source is described which provides reasonable simulations of the precession divergencies and highly transient angle of attack behavior.

Nomenclature

C_A = axial force coefficient, axial force/$\bar{q}S$
C_{l_o} = zero angle of attack rolling moment coefficient, rolling moment/$\bar{q}SD$
C_{l_p} = roll damping coefficient
C_{l_β} = distorted body rolling moment coefficient
C_m = pitching moment coefficient, $-(X_{CP}-X_{CG})C_N/D$, pitching moment/$\bar{q}SD$
C_{mo} = zero angle of attack pitching moment coefficient, contributions of asymmetry, $C_{mo_T}=[(C_{mo_z})^2+(C_{mo_y})^2]^{1/2}$
C_{m_q} = damping coefficient, Ref. $\theta D/V$
C_N = normal force coefficient, normal force/$\bar{q}S$
C_n = total out of plane moment coefficient, moment/$\bar{q}SD$
D = reference diameter, base diam
I = moment of inertia in pitch and yaw
I_x = roll moment of inertia
m = vehicle mass
M = aerodynamic moment
p, q, r = roll rate, pitch rate, yaw rate, body fixed axis
$\bar{q}$ = freestream dynamic pressure
S = reference area
t = time, from time reference
V = freestream velocity
X, Y, Z = space fixed axes which translate with the RV, but do not roll with it
q' = $\bar{q}SD$
X', Y', Z' = axes of principal inertia which are referenced to the space fixed axes by the Euler angles ψ, θ
x', y', z' = body fixed axes referenced to the X', Y', Z' axes by the Euler angle ϕ
α, β, ϕ_A = Euler angles in wind fixed coordinate system (referenced to velocity vector)
δ = $n+\phi$, orientation angle of moment asymmetry to wind vector plane
ε = magnitude of radial c.g. offset
η = orientation angle of resultant aerodynamic asymmetry moment axis to the z' axis, $\tan\eta = C_{mo_y}/C_{mo_z}$
Γ = orientation angle of radial c.g. offset to the z' axis—measured clockwise looking forward at aft end of RV
μ = $C_N I/\theta m D^2$, lift damping coefficient
ν_1 = $C_A \varepsilon \sin(\Gamma+\phi)/D$, Z' moment contribution of ε
ν_2 = $C_A \varepsilon \cos(\Gamma+\phi)/D$, Y' moment contribution of ε
θ, ψ, ϕ = Euler angles, total angle of attack, precession angle of velocity vector about X space fixed axis, roll angle of body axis. Plane fixed coordinate system

Subscripts
T = total moment about Z' *axis*
$x', y' z'$ = terms evaluated about the body fixed axes
X', Y', Z' = terms evaluated about the fixed plane axes
Derivatives with respect to time $\dot{(\ )}$
Initial conditions (6D simulations) ● ○

Introduction

ANGLE of attack anomalies observed on re-entry vehicles (RV) in the region of boundary-layer transition have been the subject of a large number of investigations over the past decade. These investigations included analyses and interpretation of flight test data,[1-4] wind tunnel tests attempting to simulate the phenomena,[5-12] and analytic methods for predicting the aerodynamic characteristics responsible for the angle of attack dynamics.[13-19] Based upon published results, the basic mechanism for the observed anomalies is not clearly established; i.e., the source may be attributed to: dynamic instability,[19] static pitching moment anomalies in the plane of the wind vector,[17] moments acting in a plane normal to the plane of the wind vector.[15]

The objective of this paper is to present an analysis technique together with flight test data which provide a basis for evaluating possible sources of the motion anomalies. Improbable sources will be identified together with evidence supporting these conclusions. A most likely source of the divergences is deduced from the "in-plane" and "out-of-plane" behavior which provides adequate simulation of detailed RV dynamics.

Method of Approach

The three degree of rotational freedom plane fixed equations of motion as applied to body fixed rate gyro information provide the basis of the analysis. Use of this coordinate system provides the benefit of separating out and resolving the dominant aerodynamic moments acting in the angle of attack plane from the

Presented as Paper 74-109 at the AIAA Aerospace Sciences Meeting, Washington, D.C., January 30–February 1, 1974; submitted February 21, 1974; revision received July 29, 1974. The author wishes to acknowledge the many contributions of S. DeLu and L. Grambsch to this paper. The timely efforts of B. Stone and R. Rowher for flight data reduction are appreciated.

Index categories: Entry Vehicle Dynamics and Control; Boundary-Layer Stability and Transition; Entry Vehicle Testing.

* Staff Engineer, Aero-Thermodynamics Department. Member AIAA.

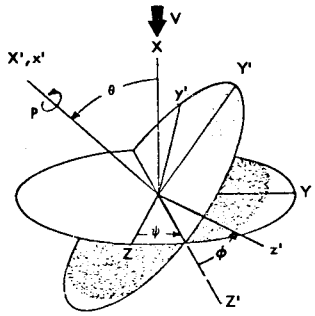

Fig. 1 Plane fixed coordinate system.

generally small moments acting in the plane normal to the angle of attack plane (out of plane). This resolution of the moments allows an in-depth evaluation of possible sources of motion anomalies observed during boundary-layer transition. The following assumptions were imposed upon the analysis: 1) constant trajectory flight path angle; 2) nonlinear aerodynamic characteristics for a basic symmetric body which are primarily functions of angle of attack; 3) an asymmetric pitching moment coefficient increment is fixed with respect to location of the body axis system over small time intervals and is independent of angle of attack; 4) a radial center of gravity (c.g.) offset is fixed in the body axis system; 5) freestream conditions (dynamic pressure, velocity, Mach number) are available as a function of time; 6) the axes for the plane fixed coordinate system (X', Y', Z') are principal axes of inertia, roll ($I_{X'}$), yaw ($I_{Y'}$), pitch ($I_{Z'}$), respectively; 7) pitch and yaw inertias are equal; 8) the aerodynamic centerline is aligned with the longitudinal inertia axis; 9) lift damping is included in a manner similar to that employed by Platus.[20]

Euler angles ψ, θ, ϕ, defining the angular motion of the RV in the plane fixed coordinate system are shown in Fig. 1. The total angle of attack ($\dot{\theta}$) motion is measured about the Z' axis in a plane which contains the velocity vector and body axis (x'); the precession motion ($\dot{\psi}$) is obtained as the motion of the angle of attack plane about the velocity vector. The angle ϕ orients the x', y', z' body axes to the angle of attack plane. Aerodynamic moments acting in this coordinate system are contained in the angle of attack plane ($M_{Z'}$), in a plane normal to the angle of attack plane ($M_{Y'}$) and about the roll axis ($M_{X'}$). The moment equations are developed from the basic relationship for the change in angular momentum in a space fixed axis system to that of a body fixed axis system.[21]

$$M_{Z'} = I\ddot{\theta} + I_x P\dot{\psi}\sin\theta - I\dot{\psi}^2\sin\theta\cos\theta = C_{mT}q' = C_m q' + q'(C_{mor}\cos\delta + v_1) - q'D(\mu - C_{m_q})\dot{\theta}/V \quad (1)$$

$$M_{Y'} = I\ddot{\psi}\sin\theta + 2I\dot{\psi}\dot{\theta}\cos\theta - I_x P\dot{\theta} = C_n q' = q'(C_{mor}\sin\delta - v_2) + q'D(\mu - C_{m_q})\dot{\psi}\sin\theta/V \quad (2)$$

$$M_{X'} = I_x\dot{P} = C_l q' = q'[C_{l_o} + C_{l_p}(PD/V) + \varepsilon\cos(\Gamma+\phi)C_N/D + C_{l_\beta}\theta\sin\delta] \quad (3)$$

Equation (2) can be re-written after multiplying by $\sin\theta$

$$Id/dt(\dot{\psi}\sin^2\theta) - I_x P\sin\theta\dot{\theta} = C_n q'\sin\theta = q'(C_{mor}\sin\delta - v_2)\sin\theta + q'D(\mu - C_{m_q})\dot{\psi}\sin^2\theta/V \quad (4)$$

Equation (4) indicates that for the assumed form of the aerodynamic moments, the precession term $I\dot{\psi}\sin^2\theta$ is directly dependent on aerodynamic damping and body fixed asymmetries, but is uncoupled from the static pitching moment and any static pitching moment asymmetries in the angle of attack plane (which may be present during boundary-layer transition). Inspection of Eq. (1) shows a strong coupling potential for significant changes in the precessing rate. Pitching moment asymmetries, if present, will directly affect the angle of attack; these effects should be discernible in the total pitching moment (C_{m_T}) derived from the flight data.

Solution of Eqs. (1) and (4) requires the time history of θ, $\dot{\theta}$, $\dot{\psi}$. These are available from the body fixed rate gyro data; however, use of flight data with inherent inaccuracies has required an additional procedure in the analysis. The three degree of freedom rate gyro integration equations for a wind fixed coordinate system[3] are employed to obtain angles α†, β†, ϕ_A. These angles are then transformed to provide the total angle of attack θ and roll position ϕ in the plane fixed coordinate system. Use of the wind fixed coordinate system allows application of the condition that the α/β motion is centered about the velocity vector during atmospheric flight; consequently small corrections can be applied to the data to null out errors caused by integration of the flight rate data. The equations used for the integration in the wind fixed coordinate system are:

$$\dot{\alpha} = (q\cos\phi_A - r\sin\phi_A) - \dot{\alpha}_c$$

$$\dot{\beta} = -\frac{1}{\cos\alpha}[(q\sin\phi_A + r\cos\phi_A)] - \dot{\beta}_c$$

$$\dot{\phi}_A = (p - \dot{\beta}\sin\alpha) \quad (5)$$

where $\dot{\alpha}_c$ and $\dot{\beta}_c$ = time variations of the apparent α/β motion center from the velocity vector and q, r, p = rates about the y', z', x' body axes of the wind fixed coordinate system. The above equations are integrated to provide α, β, ϕ_A.

The wind fixed and plane fixed coordinate systems are related through the total angle of attack and orientation of the velocity vector with respect to the body axis. Angles of attack in the wind fixed coordinate system are defined in terms of the velocity components in Fig. 2. Velocity components are $V_{X'} = V\cos\beta\cos\alpha$, $V_{Y'} = V\sin\beta$, $V_{Z'} = V\cos\beta\sin\alpha$. The angles α, β are related to the total angle of attack θ,

$$\tan^2\theta = (V_{Z'}^2 + V_{Y'}^2)/V_{X'}^2 = \tan^2\alpha + \tan^2\beta/\cos^2\alpha \quad (6)$$

where θ is also the total angle of attack in the plane fixed coordinate system (Fig. 1). The aerodynamic roll angle ϕ' (orientation of wind vector plane to the Z' axis) is determined from the velocity components

$$\tan\phi' = V_{Y'}/V_{Z'} = \tan\beta/\sin\alpha \quad (7)$$

From geometry, the velocity vector is oriented to the body axis in the two coordinate systems according to the following expression:

$$(\phi)_{\text{plane fixed}} = (\phi' + \phi_A)_{\text{wind fixed}} \quad (8)$$

The plane fixed angular rates $\dot{\theta}$, $\dot{\psi}$ are determined using Eqs. (5–7) and the body fixed rates[21]

$$\dot{\theta} = (q\cos\phi - r\sin\phi) \quad (9)$$

$$\dot{\psi} = (1/\sin\theta)(q\sin\phi + r\cos\phi) \quad (10)$$

Using the time histories of θ, $\dot{\theta}$, $\dot{\psi}$ as determined by the preceding discussion, Eqs. (1) and (4) are solved to yield the total instantaneous moment coefficients in the angle of attack plane (C_{mT}) and out of plane (C_n), respectively.

A body fixed moment asymmetry (C_{mor}) and its orientation (η) can be obtained[21] from Eq. (4) assuming that for half a cycle: C_{mor} and η are constant; the damping contribution can be neglected. The time interval is selected so that t_1 corresponds to a $\theta_{\min}$ point, t_2 to a $\theta_{\max}$ point, t_3 the next $\theta_{\min}$.

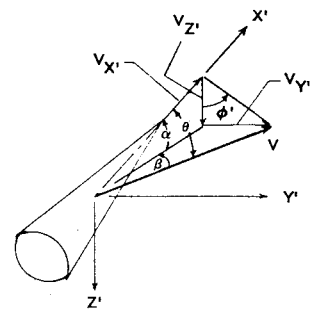

Fig. 2 Wind fixed coordinate system velocity components.

† These angles are referenced to the velocity vector. α, β, ϕ_A of the present paper correspond to θ, $-\psi$, ϕ, respectively, of Ref. 3.

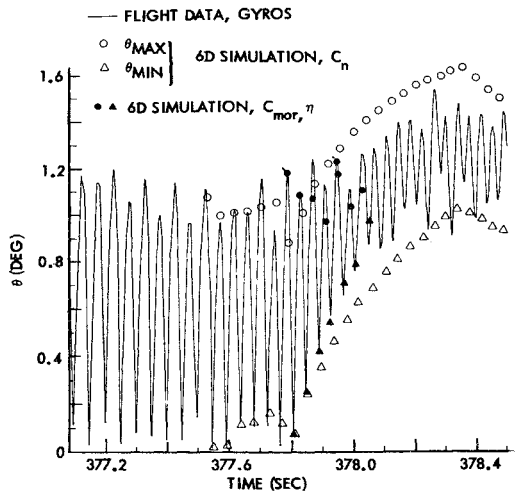

Fig. 3a Angle of attack history, RV 1.

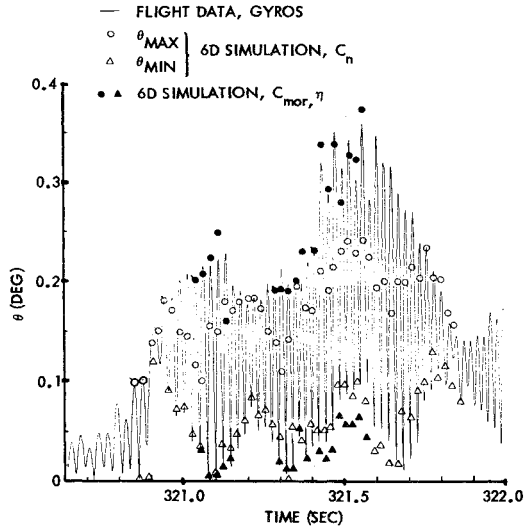

Fig. 4a Angle of attack history, RV 2.

$$\tan\eta\Big|_{t_1}^{t_3} = (-A+EC/F)/(B-EG/F) \tag{11}$$

$$C_{mor}\Big|_{t_1}^{t_3} = E/(A\cos\eta + B\sin\eta)$$

where

$$A=\int_{t_2}^{t_3} L\sin\phi\,dt \qquad B=\int_{t_2}^{t_3} L\cos\phi\,dt$$

$$C=\int_{t_1}^{t_2} L\sin\phi\,dt \qquad G=\int_{t_1}^{t_2} L\cos\phi\,dt$$

$$L=q'\sin\theta \qquad K=I\dot{\psi}\sin^2\theta + I_x P\cos\theta$$

$$E=K_{t_3}-K_{t_2}-\int_{t_2}^{t_3}[I_x\dot{P}\cos\theta - Lv_2]\,dt$$

$$F=K_{t_2}-K_{t_1}-\int_{t_1}^{t_2}[I_x\dot{P}\cos\theta - Lv_2]\,dt$$

No small angle linearizations, linear aerodynamics, or quasi-steady assumptions (constant coefficients) are imposed on the analysis.‡ The question of applicability of analyses assuming constant or slowly varying coefficients is essentially eliminated by the present technique.

Data Used

The data reported herein were obtained for 5 RV flights which were expressly instrumented to obtain detailed aerodynamic characteristics. These flights were selected based on the high quality of data (gyros and accelerometers) and distinctive dynamic behavior. Rate gyro data for all the flights were smoothed using a weighting filter.

Re-entry vehicles 1–4 employed ablative afterbodies of various materials, whereas RV 5 has a nonablating afterbody. RV4 and 5 have similar external configurations. All RVs had shape stable graphite nosetips which eliminate the uncertainty of nose contributions to the anomalies.

Boundary-layer transition (BLT) used in this report corresponds to the time period where the flow changed from laminar to fully turbulent flow conditions over the conical frustum as determined by onboard instrumentation. A summary of BLT data is shown in Table 1.

Table 1 Boundary-layer transition summary

RV Transition Times	1	2	3	4	5
Start	377.52	320.77	326.57	321.00	357.72
End	378.05	322.70	331.24	322.50	360.52

Analysis

The results to be presented consist of a relatively small, but highly transient, phase of a re-entry trajectory. Initial conditions

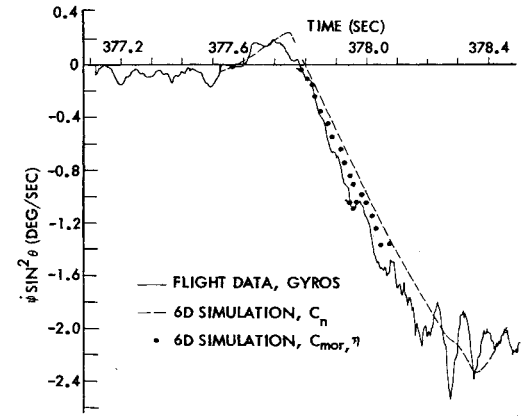

Fig. 3b Precession term history, RV 1.

‡ The exception is a body fixed moment asymmetry (trim source, which conceptually remains constant over a finite time period).

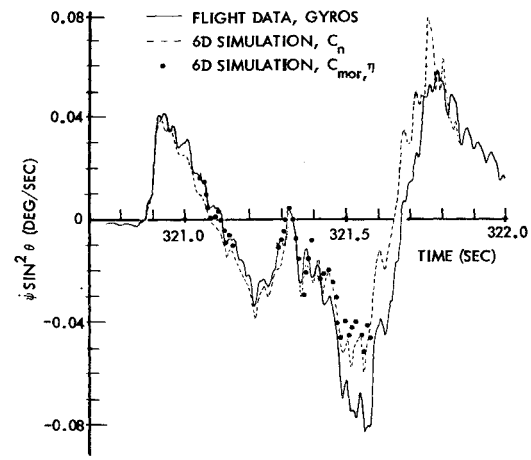

Fig. 4b Precession term history, RV 2.

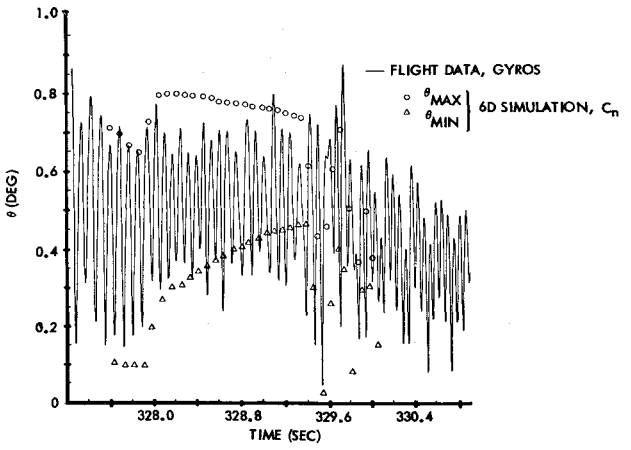

Fig. 5a Angle of attack history, RV 3.

for the succeeding analyses were the integrated results of the body fixed rates from approximately 200 kft to the time of interest. Initial conditions at 200 kft were determined by an iterative procedure for satisfying Eq. (4) at a minimum angle of attack ($\dot{\theta} = 0$) for negligible aerodynamic moments.[21]

The angle of attack and precession term histories are presented in Figs. 3–7 for all 5 flights. Boundary-layer transition for all flights was well removed (occurring more than 2 sec later) from first roll resonance effects. Note the large divergence in the magnitude and sense of the precession term for the nonablative and ablative RVs in the region of boundary-layer transition. Associated with the large excursions in the precession behavior are significant changes in the character of the motion, i.e., the ratio of maximum to minimum angle of attack.§ Subsequent sections will rely on these results to distinguish possible sources of the precession and motion anomalies from improbable considerations.

Improbable Motion Divergence Sources

Unstable Damping Coefficient

An unstable damping coefficient is not a probable source of the motion anomalies based on two criteria: the precession term cannot change signs as a result of unstable damping; large differences in "out-of-plane" and "in-plane" damping coefficients must occur at small angles of attack for an adequate representation of the motion.

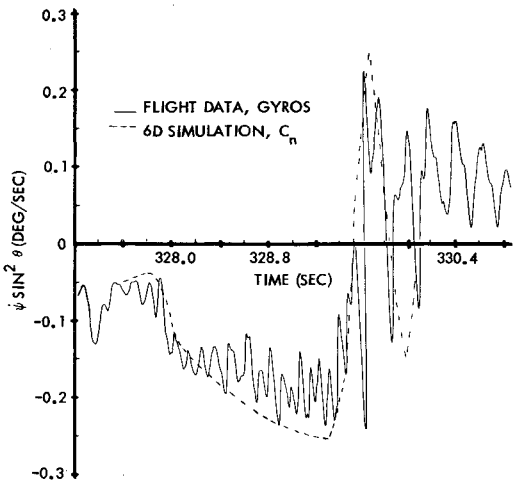

Fig. 5b Precession term history, RV 3.

§ Kirsch[19] has also demonstrated angle of attack anomalies associated with a nonablating RV.

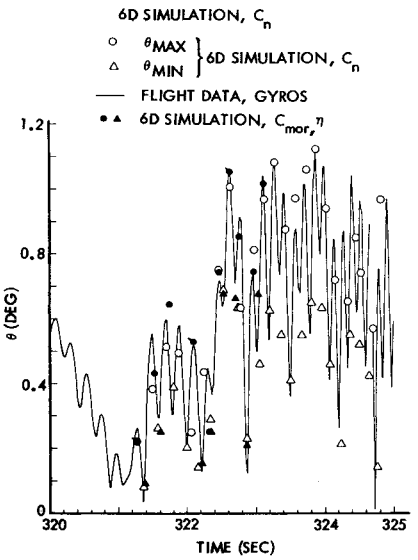

Fig. 6a Angle of attack history, RV 4.

Conditions which satisfy the first criterion are obtained from Eq. (4); this result neglects lift damping, the body fixed moment asymmetry term and the $I_x P \sin\theta\dot{\theta}$ coupling term (which was justified by the flight data).

$$-(C_{m_q})_{Y'} \approx [IV/(q'D\dot{\psi}\sin^2\theta)]\frac{d}{dt}(\dot{\psi}\sin^2\theta) \qquad (12)$$

This expression indicates that a change in sign of the precession term cannot be attributed to unstable damping unless $(C_{m_q})_{Y'} \to \infty$ as $\dot{\psi}\sin^2\theta \to 0$. Referring to the precession term histories in Figs. 3–7, all of the flights exhibit instances of the precession term changing signs, with RV 2 and 3 repeating this characteristic five times during boundary-layer transition. This precession term behavior was verified with accelerometer data.

The second criterion is demonstrated by simulations of the RV dynamics with various damping coefficients. An "implied" damping coefficient, shown in Fig. 8a, was derived for RV1 from Eq. (4) for conditions where damping could be a plausible consideration. The 6D results, shown in Fig. 8b with equal dynamic stability terms, indicate a large overshoot in the maximum angle of attack and undershoot of the minimum angle compared to flight values. A second 6D simulation, presented in Fig. 8b using the "implied" damping for $(C_{m_q})_{Y'}$ and a value of $(C_{m_q})_{Z'} = -0.78$ for the in-plane damping,[22] show reasonable agreement with the changes in the flight motion characteristics. The motion divergence demonstrated for this

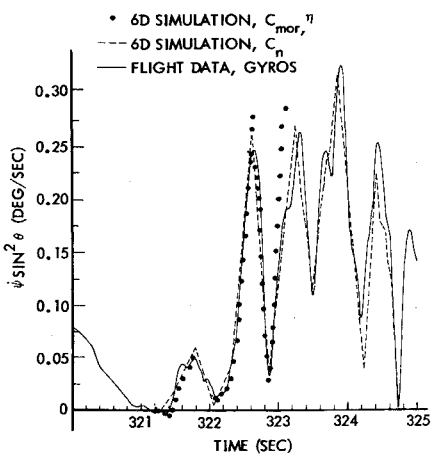

Fig. 6b Precession term history, RV 4.

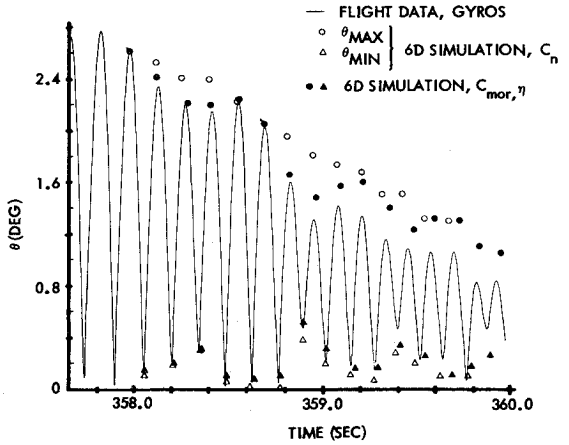

Fig. 7a Angle of attack history, RV 5.

flight is primarily a coupling effect of the precession rate (Eq. 1) resulting from "out-of-plane" moments. Consequently, assuming the divergence in the precession term is a result of an unstable damping coefficient requires a vastly different (stable) "in-plane" damping coefficient to duplicate the motion. Similar characteristics could be demonstrated for RV 3 and 4.

Out-of-Plane Static Moment

A static moment acting in the plane normal to the wind vector plane ("out-of-plane") was next considered as a probable contributor. The total "out-of-plane" moment (C_n) obtained from Eq. (4), was approximated for use in 6D dynamic simulations. Predicted aerodynamic characteristics[22] for the "in-plane" and trajectory effects were used together with averages of the flight derived static pitching moment coefficient characteristics in the simulations. Roll moments were included to produce the flight spinup results for RV 3; all other flights used constant roll rates.

Precession term histories obtained from the 6D simulations are compared to the flight values in Figs. 3b–7b as an indication of the approximations used in the results. 6D angle of attack results compared to the flight values in Figs. 3a through 7a, show relatively good simulation of the overall angle of attack magnitude and change of the motion characteristics for RVs 1, 3, and 4. These results would imply that the "out-of-plane" moment is the dominant source of the motion anomalies observed during boundary-layer transition, substantiating the conclusions reached by Waterfall.[15] However, 6D angle of attack simulations for RV 2 show significant disagreement in regions where the sense of the precession term is changing. Large

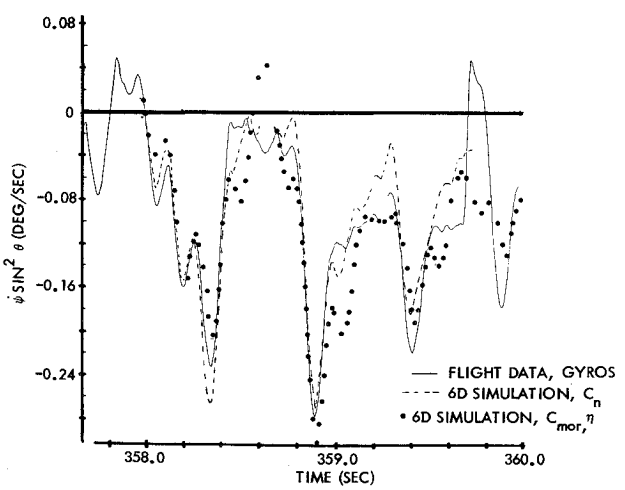

Fig. 7b Precession term history, RV 5.

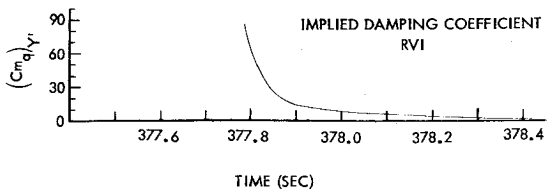

Fig. 8a Implied damping coefficient history.

step changes in θ for RV 2 and RV 5 (Fig. 7a) are noted in the flight data, but are not obtained in the 6D simulations. Although the gross angle of attack behavior is demonstrated with an out-of-plane moment, significant in-plane moment contributors are apparent in the results for these two RVs.

In-Plane Moment Asymmetries

Although "in-plane" moment asymmetries are not responsible for the observed precession divergencies, this contribution can be combined with "out-of-plane" asymmetries to produce the motion and precession of anomalies. Interpretation of the resultant moment asymmetries acting on an RV is a difficult task; these effects can be attributed to: 1) a wind fixed source (dependent primarily on angle of attack where transition asymmetries are realized in both the wind vector plane and out of plane orientations¶); 2) a body fixed source. The following section indicates the criteria used to select the body fixed source as the logical choice compared to the wind fixed moment possibility.

Source of Divergencies

Body Fixed Moment Asymmetry

The full paper contained total in-plane moment data which indicated distinct body fixed moment asymmetries for RVs 2 through 5 over finite time periods. An independent evaluation of a body fixed source, obtained by applying Eq. (11) to the precession term behavior, produced moment asymmetries which generally agreed in magnitude with those deduced from the total in-plane moments. Consequently, a transient body fixed moment asymmetry which could produce both the "in" and "out" of plane moment components was considered as the primary source of the abnormal RV behavior.

Body fixed moment asymmetries (C_{mor}) and orientation angles (η) derived from the gyro results, Eq. (11), exhibited a high degree of variability during the period of BLT. This behavior was compared in the full paper with trim moment results obtained with a low frequency filtering method applied to accelerometer data. Reasonable agreement between the two techniques was demonstrated for RVs 4 and 5, where the

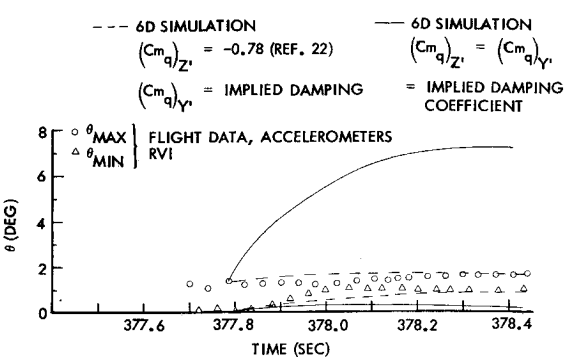

Fig. 8b θ histories for various damping assumptions, RV 1.

¶ This type of transition asymmetry has been observed in wind tunnel tests of transition studies on slender cones at hypersonic speeds.[23]

orientation angle was slowly changing. Relatively poor agreement was realized for RVs 1–3, where the gyro technique provided highly transient behavior for C_{mor} and η compared to slowly changing behavior for the accelerometer derived results.

Simulations Using Body Fixed Moment

Smoothed results of the body fixed moment asymmetry terms obtained from the precession behavior were utilized in 6D simulations to assess the validity of these terms to describe the RV dynamics. Average pitching moment coefficient curves derived from the flight in-plane moment results were used together with predicted dynamic stability characteristics.[22] The 6D results obtained using C_{mor}, η (filled symbols in Figs. 3–7) were highly sensitive to phasing effects; consequently, valid data consisted of brief time intervals from selected initial conditions.

The 6D angle of attack results are compared to the RV 1 flight values in Fig. 3a for $378.05 > t > 377.78$; the precession term behavior is compared in Fig. 3b. Reasonable agreement is noted for the angle of attack history, particularly the $\theta_{\min}$ values; the significant precession term divergence is well simulated by a highly transient small moment asymmetry. Angle of attack and precession results obtained for the RV 2 flight are compared in Figs. 4a and 4b, respectively. The first segment of time for $321.15 > t > 321.04$ encompasses the region where the precession term is rapidly changing from the positive to negative mode; good simulation of the flight results is indicated. The corresponding angle of attack history shows reasonably good agreement in trend with the flight data as contrasted to the results employing an out-of-plane moment. Similar results are obtained for the time period $321.38 > t > 321.29$, where the precession term is again rapidly changing modes. The time period $321.57 > t > 321.41$ includes the region where relatively large, highly transient C_{mor} results were input. Reasonable precession term behavior was obtained with the simulation; good angle of attack results were obtained including the step change in $\theta_{\max}$ at $t = 321.43$, together with "beating" of the $\theta_{\max}$ points.

The 6D angle of attack results are compared to RV 4 flight results in Fig. 6a for $323.1 > t > 321.25$; the precession term results are shown in Fig. 6b. Reasonably good agreement is obtained for both the highly transient angle of attack and precession term histories. Results for RV 5, shown in Figs. 7a and 7b indicate good simulation of the precession term behavior. Good agreement is demonstrated for the angle of attack behavior, including the large step change in $\theta_{\max}$ at 358.84. The characteristic "beating" of the $\theta_{\max}$ envelope is demonstrated by this simulation as opposed to the out of plane results.

Conclusions

Simulations obtained with a relatively small, but highly transient body fixed moment source (derived from the precession characteristics) demonstrated the significant divergences observed in the flight precession term and angle of attack results. Increased outgassing for a peripheral segment of an ablative heat shield (for finite time periods) in response to boundary-layer transition asymmetries is the postulated mechanism for the body fixed moments. Thermal distortion associated with asymmetric transition (and heating) is the postulated mechanism for the body fixed moments experienced by the nonablative RV.

References

[1] Pettus, J. J., "Re-Entry Vehicle Flight Test Dynamic Stability Analysis I," *Transactions of the Second Technical Workshop on Dynamic Stability Testing*, Paper 1, Vol. I, 1965, Arnold Air Force Station, Tenn.

[2] Ross, R. F., "Determination of Static and Dynamic Aerodynamic Characteristics of Re-Entry Vehicles from Dynamic Motion Data," *Transactions of the 3rd Technical Workshop on Dynamic Stability Problems*, Paper 8, Vol. III, 1968, NASA Ames Research Center, Moffett Field, Calif.

[3] Ferro, J. M., "Free Flight Determination of Dynamic Stability," *Transactions of the 2nd Technical Workshop on Dynamic Stability Testing*, Paper 2, Vol. III, 1965, Arnold Air Force Station, Tenn.

[4] Burton, T. D. and Lamour, R. A., "A Method for Extracting the Dynamic Damping Coefficient from Flight Test Lateral Rate Data," AIAA Paper 71-49, New York, 1971.

[5] Colosimo, D. D., "Mass Transfer-Dynamic Stability Testing in the Wave Superheater Hypersonic Tunnel," *Transactions of the 2nd Technical Workshop on Dynamic Stability Testing*, Paper 2, Vol. I, 1965, Arnold Air Force Station, Tenn.

[6] Stalmach, C. J., "Stability Investigations during Simulated Ablation in a Hypervelocity Wind Tunnel," *Transactions of the 2nd Technical Workshop on Dynamic Stability Testing*, Paper 3, Vol. I, 1965, Arnold Air Force Station, Tenn.

[7] Hobbs, R. B., "Ground Test Simulation of Flight Instability," *Transactions of the 2nd Technical Workshop on Dynamic Stability Testing*, Paper 4, Vol. I, 1965, Arnold Air Force Station, Tenn.

[8] Stalmach, C. J. and Lindsey, J. L., "Effects of Oscillatory Mass Addition on Boundary Layer Pressure and Vehicle Stability," *Transactions of the 3rd Technical Workshop on Dynamic Stability Problems*, Paper 12, Vol. I, 1968, NASA Ames Research Center, Moffett Field, Calif.

[9] Sacks, I. and Shurman, E. E., "Aerodynamic Phenomena Associated with Advanced Reentry Systems," AVCO-RAD-TM 63-79, Oct. 1963, Avco Corp., Wilmington, Mass.

[10] Chrusciel, G. T., Chang, S. S., "Effects of Ablation on Hypersonic Aerodynamic Stability Characteristics," AIAA Paper 66-410, Los Angeles, Calif., 1966.

[11] Grimes, J. H., Jr. and Casey, J. H., "Influence of Ablation on the Dynamics of Slender Re-Entry Configurations," *Journal of Spacecraft and Rockets*, Vol. 2, No. 1, Jan.–Feb. 1965, pp. 106–108.

[12] Ward, L. K., "Influence of Boundary Layer Transition on Dynamic Stability at Hypersonic Speeds," *Transactions of the 2nd Technical Workshop on Dynamic Stability Testing*, Paper 6, Vol. II, 1965, Arnold Air Force Station, Tenn.

[13] Ericsson, L. E. and Reding, J. P., "Ablation Effects on Vehicle Dynamics," *Journal of Spacecraft and Rockets*, Vol. 3, No. 10, Oct. 1966, pp. 1476–1483.

[14] Ericsson, L. E., "Effect of Boundary-Layer Transition on Vehicle Dynamics," *Journal of Spacecraft and Rockets*, Vol. 6, No. 12, Dec. 1969, pp. 1404–1409.

[15] Waterfall, A. P., "Effect of Ablation on the Dynamics of Spinning Re-Entry Vehicles," *Journal of Spacecraft and Rockets*, Vol. 6, No. 9, Sept. 1969, pp. 1038–1044.

[16] Martellucci, A., "Asymmetric Transition Effects on the Static Stability and Motion History of a Slender Vehicle," TR-70-141, 1970, Space and Missiles Systems Organization, U.S. Air Force.

[17] Martellucci, A. and Neff, R. S., "Influence of Asymmetric Transition on Re-Entry Vehicle Characteristic," *Journal of Spacecraft and Rockets*, Vol. 8, No. 5, May 1971, pp. 476–482.

[18] Ericsson, L. E., "Transition Effects on Slender Vehicle Stability and Trim Characteristics," AIAA Paper 73-126, Washington, D.C., 1973.

[19] Kirsch, A. A., "A Proposed Dynamic Stability Solution," AIAA Paper 73-180, Washington, D. C., 1973.

[20] Platus, D. H., "Angle-of-Attack Convergence and Windward-Meridian Rotation Rate of Rolling Re-Entry Vehicles," *AIAA Journal*, Vol. 7, No. 12, Dec. 1969, pp. 2324–2330.

[21] Chrusciel, G. T., "Application of Plane Fixed Equations of Motion to Re-Entry Vehicle Flight Analysis," TM 81-11/69, Aug. 1972, Lockheed Space and Missile Co., Sunnyvale Calif.

[22] Chrusciel, G. T. and Hull, L. D., "Theoretical Method for Calculating Aerodynamic Characteristics of Spherically Blunted Cones," AIAA Paper 68-674, Los Angeles, Calif., 1968.

[23] DiChristina, V., "Three-Dimensional Laminar Boundary-Layer Transition on a Sharp 8° Cone at Mach 10," *AIAA Journal*, Vol. 8, No. 5, May 1970, pp. 852–856.